



# Isothermal and thermal cycling oxidation of hot-dip aluminide coating on flake/spheroidal graphite cast iron

Meng-Bin Lin <sup>a,\*</sup>, Chaur-Jeng Wang <sup>a</sup>, Alex A. Volinsky <sup>b</sup>

<sup>a</sup> Department of Mechanical Engineering, National Taiwan University of Science and Technology, Taipei, Taiwan

<sup>b</sup> Department for Mechanical Engineering, University of South Florida, Tampa FL 33620, USA

## ARTICLE INFO

Available online 17 June 2011

### Keywords:

Hot-dip Al  
Flake graphite cast iron  
Spheroidal graphite cast iron  
High-temperature oxidation

## ABSTRACT

Two types of cast iron, flake graphite and spheroidal graphite cast iron, with ferrite matrix and similar composition, were aluminized by hot-dipping. As-coated aluminide layer consists of the outer Al topcoat, inner Fe–Al intermetallic layer and dispersed graphite. Isothermal and thermal cycling oxidation tests of aluminized specimens have been conducted. Cast irons with aluminide coating exhibit higher oxidation resistance than without the coating. However, different graphite structure results in diverse quality of aluminide coatings. Aluminide coating on flake graphite cast iron exhibits less oxidation resistance and adhesion to the substrate.

© 2011 Elsevier B.V. All rights reserved.

## 1. Introduction

Flake and spheroidal graphite cast irons have excellent castability, high damping, good machinability and relatively low cost compared with alloy steels with similar mechanical properties. Both irons are used as engineering materials in high temperature applications, such as furnace parts, turbocharger housings and exhaust manifolds that require high-temperature oxidation resistance and mechanical strength [1–6].

In recent years, increased engine efficiency, together with decreased exhaust gas pollutant emissions, have pushed automobile manufacturers to raise maximum combustion temperature and therefore exhaust gas temperature in engines. As a result, exhaust gas corrosive effect is enhanced, leading to rapid oxidation of cast iron [7].

Hot-dip aluminizing of mild and stainless steels is widely used to improve their oxidation and corrosion resistance [8–10]. However, aluminide coatings on flake or spheroidal graphite cast iron are not as common. Consequently, in the present work, flake and spheroidal graphite cast iron have been aluminized by hot-dipping, and then their oxidation and thermal fatigue resistance were evaluated. Finally, the effect of graphite structure on oxidation resistance of aluminide coatings on cast irons was investigated.

## 2. Experimental procedure

Two commercial materials were used in this study: FC200 (ferritic flake graphite cast iron) and FCD400 (ferritic spheroidal graphite cast iron), which microstructure as presented in Fig. 1(a)–(b). Both cast irons were provided by Yongzhen Co., Ltd, Taiwan. Chemical composition of both cast irons was analyzed by glow discharge spectrometer (LECO, GDS-750A, Germany) as shown in Table 1.

Rectangular specimens were cut into 10 mm × 10 mm × 2 mm pieces and polished with grit paper to 800 grade. Specimens for further hot-dip treatment were drilled and hung by stainless wires, then cleaned ultrasonically in alkaline, acid, and acetone solutions. To achieve full contact between specimens and molten aluminum, specimens were immersed in an aqueous flux solution and dried before aluminizing. The flux mainly consisted of KCl, LiCl and Na<sub>2</sub>SiF<sub>6</sub>. After fluxing, specimens were hung in a step-motor-controlled feeder and immersed in a molten aluminum bath (Al > 99.9 wt.%) at 700 °C for 120 s with 15 cm/min up and down immersion. Hot-dipped specimens were cleaned in mixed aqueous solution of nitride acid, phosphoric acid, and water with 1:1:1 volume fraction at 25 °C.

Oxidation and thermal fatigue resistance of hot-dip aluminide coatings on flake and spheroidal cast irons were determined by isothermal and thermal cycling oxidation tests. Aluminized specimens were placed in isothermal and automatically heating–cooling furnace, respectively. Isothermal oxidation tests were conducted at 750 °C in static air for 4 to 192 h. After isothermal oxidation tests, specimens were cooled in air and their mass was measured. Oxidized specimens mass were measured with a precision electronic balance (0.1 mg accuracy), and the value of weight change per unit

\* Corresponding author. Tel.: +886 2 27376441; fax: +886 2 27376460.  
E-mail address: [d9603506@mail.ntust.edu.tw](mailto:d9603506@mail.ntust.edu.tw) (M.-B. Lin).

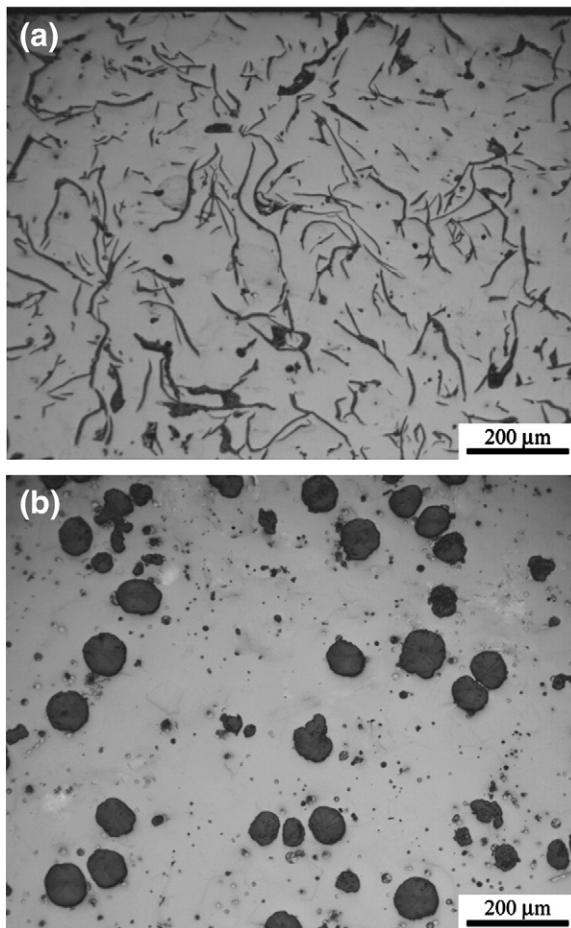


**Fig. 1.** OM micrographs of cast iron: (a) FC200 flake graphite cast iron (ferrite matrix and graphite flakes); (b) FCD400 spheroidal graphite cast iron (ferrite matrix and graphite spheroids).

area was averaged from four specimens under each experimental conditions.

Cyclic oxidation tests were conducted over a period of 96 cycles. Each cycle consisted of 60 min at 750 °C and 60 min at room temperature, which was long enough to cool the specimens below 30 °C.

Cyclic oxidation behavior was evaluated by the weight change, measured with a precision electronic balance (0.1 mg accuracy). The weight change of cyclic oxidation specimens excluded the oxide scale that spalled off during heating or cooling.

The phase structure of aluminized and oxidized specimens was identified by X-ray diffraction (XRD) using monochromatic Cu-K $\alpha$  radiation operated at 40 kV and 100 mA. The surface morphology and cross-sections of specimens were examined using scanning electron microscopy (SEM) with energy-dispersive spectrometry (EDS) and electron-probe microanalysis (EPMA).

### 3. Results and discussion

#### 3.1. Microstructure of the as-coated aluminide layer

Optical cross-sectional micrographs of as-coated flake/spheroidal graphite cast iron are presented in Fig. 2(a)–(b). After hot-dipping in

**Table 1**  
Chemical composition of flake and spheroidal graphite cast irons (wt.%).

Alloy	C	Si	Mn	P	S	Cr	Ni	Mo	Cu	Fe
FC200	2.95	1.53	1.01	0.04	0.01	0.19	0.03	0.05	0.08	Balance
FCD400	2.22	2.55	0.24	0.01	0.00	0.15	0.02	0.04	0.01	Balance

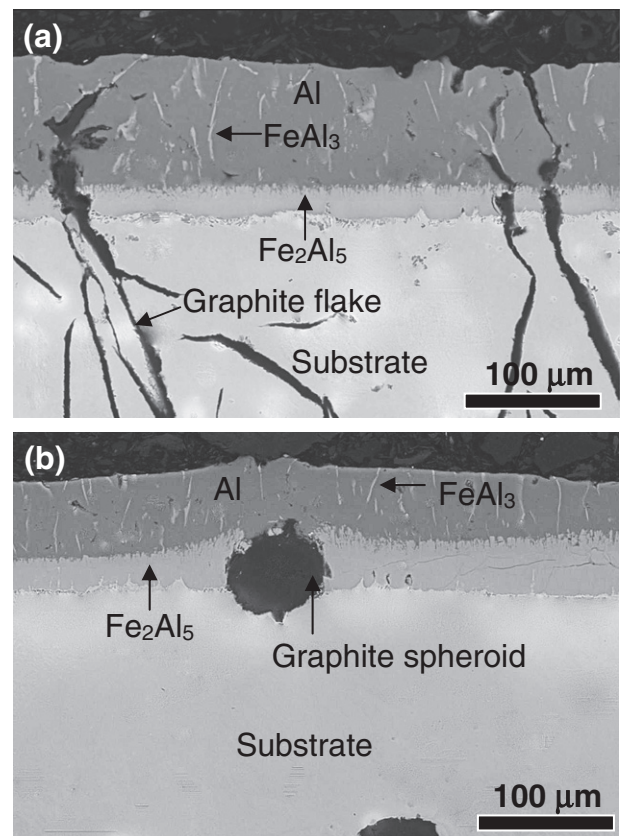


**Fig. 2.** The micrographs of cross sections of aluminized cast irons obtained by SEM: (a) aluminized FC200; (b) aluminized FCD400.

Al for 120 s, the overall thickness of aluminide layer is 80  $\mu\text{m}$ . The aluminide coating consist of the outer Al topcoat, inner Fe–Al intermetallic layer and dispersed graphite. EDS and XRD analysis revealed that there are  $\text{FeAl}_3$  and  $\text{Fe}_2\text{Al}_5$  intermetallic phases present in the as-coated aluminide layer.  $\text{FeAl}_3$  intermetallic phase is rod-shaped, dispersed in the Al topcoat.  $\text{Fe}_2\text{Al}_5$  intermetallic phase grows continuously rather than form columnar-grain layer adjacent to the substrate. Compared with Kobayashi's work [8], in which the interface between  $\text{Fe}_2\text{Al}_5$  layer and mild steel substrate is fairly irregular (tongue-like) due to fast and preferential  $\text{Fe}_2\text{Al}_5$  growth, in this study the interface between  $\text{Fe}_2\text{Al}_5$  and cast iron substrate is smoother. This difference may be caused by Si addition to the cast iron substrate. It is generally recognized that Si reduces the rate of Al solid state diffusion in steel, which may inhibit  $\text{Fe}_2\text{Al}_5$  growth [11–13].

Besides, graphite in the substrate could be deemed markers and affect aluminide layer morphology during hot-dip immersion in Al. Fe–Al inter-diffusion promotes intermetallic phase growth, while graphite blocks intermetallic Fe–Al phase formation during hot-dipping process. Thus, some regions of substrate are not covered with  $\text{Fe}_2\text{Al}_5$  intermetallic phase, as shown in Fig. 2(a)–(b). Since Fe diffusion rate is faster than that of Al [8], aluminide layer gradually grows inward (reducing the substrate thickness), that is, graphite would gradually be trapped in aluminide layer during hot-dipping in Al melt. Finally, as a result of hot-dipping in Al, graphite exists in aluminide layers as well as in the cast iron substrate, as shown in Fig. 2(a)–(b). Therefore, microstructure of aluminide coating on FC200 is different from that on FCD400 in flake/spheroidal graphite distribution. The effect of graphite flakes and spheroids on the oxidation resistance of aluminide layer has not been reported yet, and will be explored and discussed in the following sections.

### 3.2. High-temperature oxidation kinetics

Oxidation kinetics of aluminide coatings was investigated at 750 °C in static air, and the rates of weight gain per surface area with and without coating are plotted against time in Fig. 3(a)–(b). Oxidation kinetics of aluminide coating (Fe–Al intermetallics) is often describes by Wagner's equation with a parabolic law of oxide growth:

$$\Delta m^2 = k_p t \quad (1)$$

where  $\Delta m$  is the surface specific weight change,  $t$  is the oxidation time and  $k_p$  is a parabolic constant [14,15]. The value of parabolic constants of specimens can be derived from the Eq. (1) and

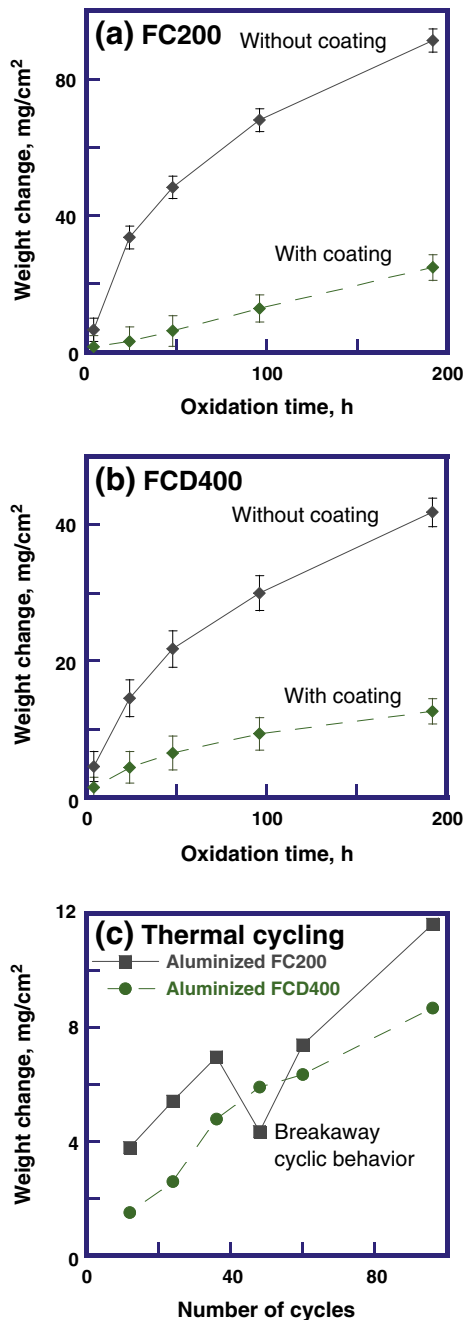


**Fig. 3.** Oxidation kinetics at 750 °C in air: (a) flake graphite cast iron with and without aluminide coating; (b) spheroidal graphite cast iron with and without aluminide coating; (c) thermal cycling oxidation of aluminized FC200 and FCD400.

corresponding oxidation results (Fig. 3(a)–(b)), as listed in Table 2. High-temperature oxidation resistance can be evaluated with the parabolic constants. The benefit of cast iron hot-dipping in Al is significant improvement of the high-temperature oxidation resistance signified by much lower parabolic constant. Although coating parameters of both cast irons are similar, parabolic constant of aluminized FC200 is greater than that of aluminized FCD400 by an order of magnitude. This signifies that the hot-dip aluminide coating cannot completely overcome extensive oxidation occurred in aluminized FC200 specimens.

Since the hot-dip aluminide layer is relatively thick (~80 μm), the problem of aluminide layer spallation resulted from thermal stress relief. Therefore, thermal cycling tests were conducted (Fig. 3(c)). The weight change of specimens exposed to thermal cycling reveals the adhesion of the aluminide layer to cast irons. After 48 thermal cycles, aluminized FC200 exhibited breakaway cyclic behavior with spallation of oxide/aluminide layer. In contrast aluminide coating exhibited better adhesion to FCD400. After 96 thermal cycles, no significant weight loss was detected and visual inspection indicated that aluminide coating still adhered to the substrate.

### 3.3. Microstructure of aluminide layer after oxidation test

In order to understand why the hot-dip aluminide coating on FC200 exhibited lower oxidation resistance and adhesion, microstructure of aluminized FC200 after oxidation test was investigated, presented in Fig. 4(a)–(e).

Aluminide layer phase composition is transforming, due to Al inward diffusion into the substrate resulting from chemical composition gradient [16]. Therefore, Al topcoat is consumed and the intermetallic layer consists of low Al composition FeAl<sub>2</sub> phase (Fig. 4(a)–(b)).

Although Al concentration is diluted, it is still higher than the critical 3.9 at.% value to form aluminum oxide [17]. XRD analysis confirmed the formation of α-alumina on the surface of aluminized FC200 and FCD400 specimens after 750 °C oxidation test for 192 h.

Extensive oxidation of aluminized FC200 is observed. As presented in Fig. 4(e), the area of aluminide layer is free from flake graphite; while iron oxide is observed instead. According to thermodynamics and literature data [18,19], it is known that during 750 °C air exposure graphite would directly interact with oxygen causing graphite oxidation ( $2C + O_2 \rightarrow 2CO$  or  $C + O_2 \rightarrow CO_2$ ), leaving cracks or pores in the aluminide layer which results in oxygen penetration through aluminide coating to the cast iron substrate. Consequently, different graphite structure is the reason for diverse oxidation behavior of aluminide coating. The structure of flake graphite in the aluminide layer and the substrate is extended and connected, producing continuous pass, allowing oxygen penetration through the aluminide coating to cast iron substrate, initiating oxygen attack. Thus, severe iron oxide grew and broke through the aluminide coating following cracks (see Fig. 4(c)–(d)). Although iron oxide formed, oxygen access to cast iron substrate was not inhibited. After long-term exposure, subsurface oxidation is observed, as shown in Fig. 4(d). Consequently, severe iron oxide growth and subsurface oxidation led to significant

**Table 2**

Parabolic rate constants for the oxidation of cast irons without and with coating at 750 °C.

Alloy	Without coating			With coating		
	mg <sup>2</sup>	cm <sup>-4</sup>	s <sup>-1</sup>	mg <sup>2</sup>	cm <sup>-4</sup>	s <sup>-1</sup>
FC200	13.45 × 10 <sup>-3</sup>			1.09 × 10 <sup>-3</sup>		
FCD400	2.70 × 10 <sup>-3</sup>			2.30 × 10 <sup>-4</sup>		

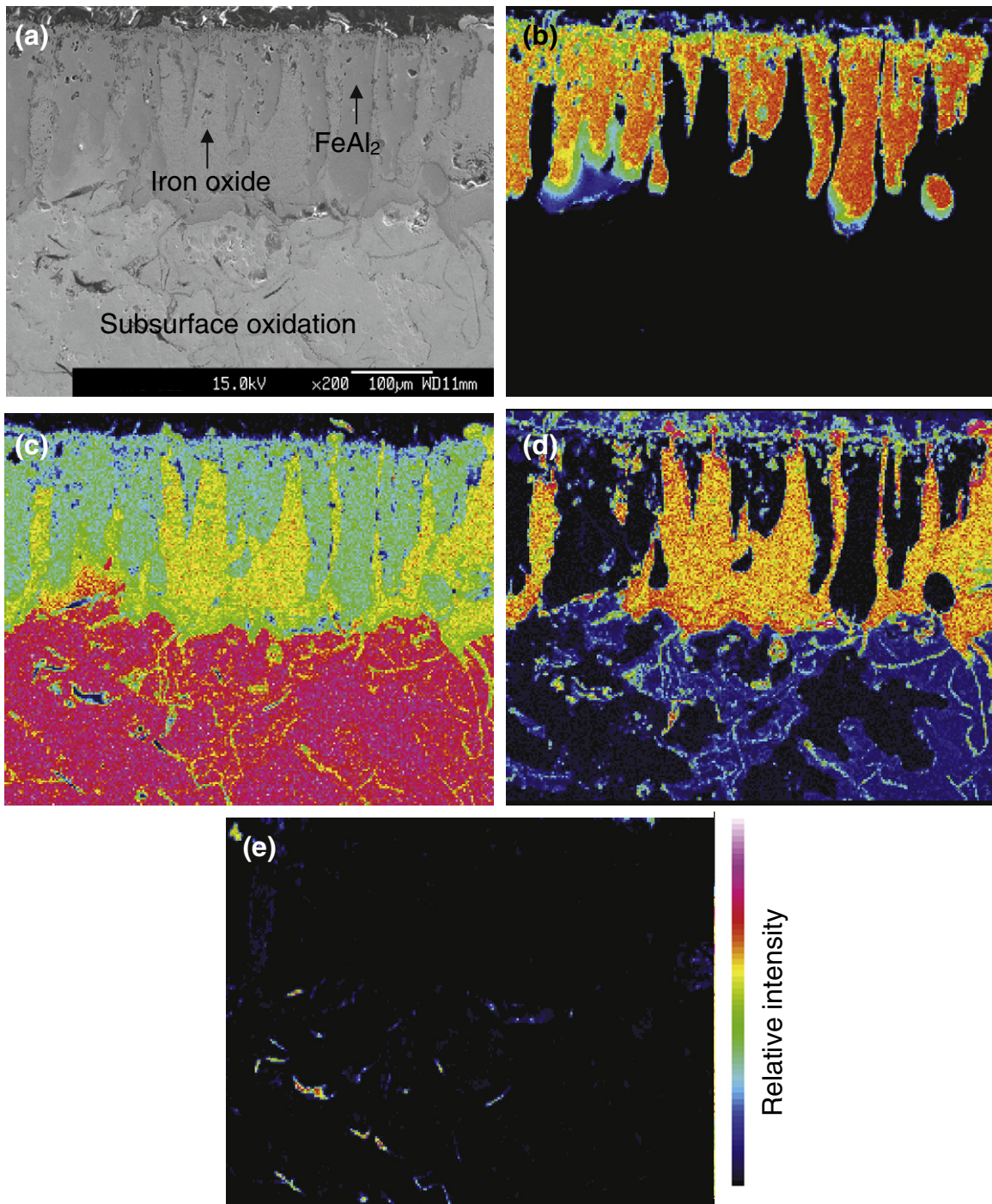


**Fig. 4.** EPMA analysis showing the element distribution map of aluminized FC200 after 750 °C oxidation test for 96 h; (a) BEI micrograph of cross section of aluminized FC200 exposed for 96 h in air at 750 °C; (b) Al element distribution map; (c) Fe element distribution map; (d) O element distribution map; (e) C element distribution map.

increase in the weight gain of oxidation kinetics of aluminized FC200 (see Fig. 3(a)).

Spallation of aluminide coating from the flake graphite cast iron (Fig. 3(c)) may result from severe iron oxide formation during thermal cycling oxidation test. Based on the Pilling–Bedworth ratio theory [20] (PBR: the ratio of the volume of oxide per metal ion to the volume of metal per metal atom), the PBR value of iron oxides is greater than 1 (PBR of FeO, Fe<sub>3</sub>O<sub>4</sub> and Fe<sub>2</sub>O<sub>3</sub> are 1.78, 2.10 and 2.14, respectively), which reveals that formation of iron oxides induce significant stress due to volume expansion. When strain energy release rate due to

thermal and volume expansion stresses exceeds interfacial toughness, aluminide coating spalls from the substrate, as seen in Fig. 3(c), where aluminized FC200 exhibits breakaway cyclic behavior.

After 750 °C isothermal and thermal cycling oxidation for 96 h and 60 cycles, aluminized FCD400 specimens were examined with SEM, revealing slight oxidation and aluminide layer still adhered to the cast iron substrate, as seen in Fig. 5(a)–(b). Since spheroidal graphite precipitation is separated and extended, that connected penetration passage is absent in the aluminide layer. This resulted in that aluminide coating on spheroidal graphite cast iron exhibits better

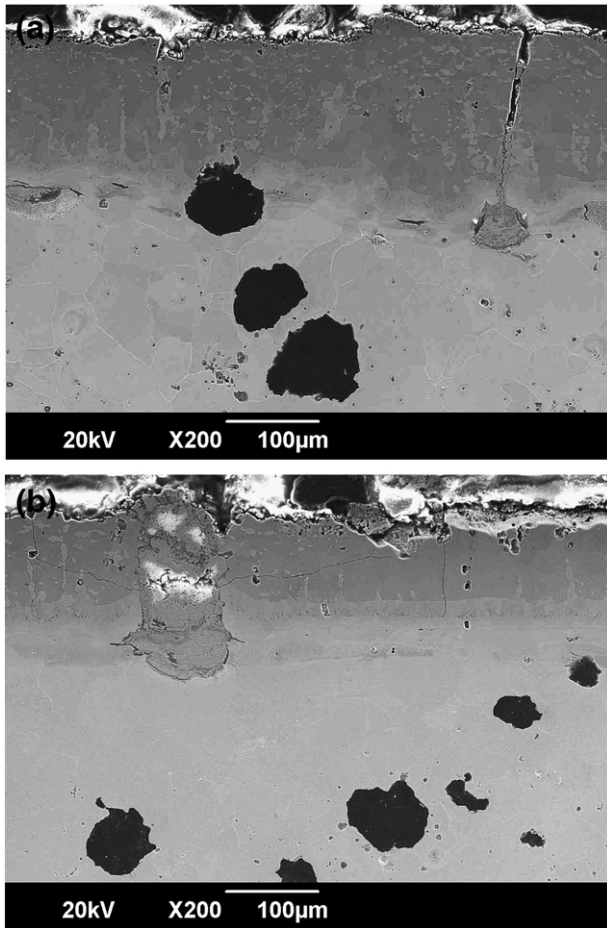


Fig. 5. SEM micrographs of cross sections of aluminized FCD400 (a) after 750 °C oxidation test for 96 h and (b) after thermal cycling for 60 cycles.

oxidation resistance; less oxidation and good adhesion observed in aluminized FCD400 specimen.

#### 4. Conclusions

Two types of cast iron, flake graphite (FC200) and spheroidal graphite cast iron (FCD400), with ferrite matrix and similar com-

position, were aluminized by hot-dipping. As-coated aluminide layer on cast irons consists of outer Al topcoat, inner Fe–Al intermetallic layer ( $\text{FeAl}_3$  and  $\text{Fe}_2\text{Al}_5$ ) and dispersed flake/spheroidal graphite. Graphite in cast iron blocks Fe–Al intermetallic phase formation during hot-dipping process, since some regions of substrate were not covered with  $\text{Fe}_2\text{Al}_5$  intermetallic phase.

High-temperature oxidation resistance of cast irons was improved with aluminide coating. However, different graphite structure results in diverse quality of aluminide coatings. Flake graphite dispersed in aluminide layer directly interacts with oxygen causing graphite oxidation ( $2\text{C} + \text{O}_2 \rightarrow 2\text{CO}$  or  $\text{C} + \text{O}_2 \rightarrow \text{CO}_2$ ), then cracks propagate along the flake graphite, providing continuous passage to allow oxygen penetration through aluminide coating to the cast iron substrate, initiating oxygen attack. Consequently iron oxide grew through aluminide layer and severe subsurface oxidation occurred. The oxidation kinetics proved that the aluminide coating on spheroidal graphite cast iron exhibits good high-temperature oxidation resistance and adhesion to the substrate.

#### Acknowledgement

The authors acknowledge support from the National Science Council of Republic of China under grant NSC 99-2221-E-011-014-MY3.

#### References

- [1] P. Curcio, B. Kerezi, P. Brown, *J. Mater. Sci.* 34 (1999) 4775.
- [2] C. Labrecque, M. Gagne, *Can. Metall. Quart* 37 (1998) 343.
- [3] G.S. Cho, K.H. Choe, K.W. Lee, A. Ikenaga, *Mater. Sci. Technol.* 23 (2007) 97.
- [4] A.R. Ghaderi, M. Nili Ahmadabadi, H.M. Ghasemi, *Wear* 225 (2003) 410.
- [5] M. Hatate, T. Shoitto, N. Takahashi, K. Shimizu, *Wear* 251 (2001) 885.
- [6] Y. Zhang, Y. Chen, R. He, B. Shen, *Wear* 166 (1993) 179.
- [7] Yang Yun Long, Cao Zhan Yi, Qi Yang, Liu Yong Bing, *Adv. Mater. Res.* 97 (101) (2010) 530.
- [8] S. Kobayashi, T. Yakou, *Mater. Sci. Eng. A* 338 (2002) 44.
- [9] T.L. Hu, H.L. Huang, D. Gan, T.Y. Lee, *Surf. Coat. Technol.* 201 (2006) 3502.
- [10] C.J. Wang, C.C. Li, *Surf. Coat. Technol.* 37 (2003) 177.
- [11] R.W. Richards, R.D. Jones, P.D. Clements, H. Clarke, *Int. Mater. Rev.* 39 (1994) 191.
- [12] G. Eggeler, W. Auer, H. Kaesche, *J. Mater. Sci.* 21 (1986) 3348.
- [13] G.M. Bedford, J. Boustead, *Met. Technol.* 1 (5) (1974) 233.
- [14] N. Babu, R. Balasubramaniam, A. Ghosh, *Corros. Sci.* 43 (2001) 2239.
- [15] C. Badini, F. Laurella, *Surf. Coat. Technol.* 135 (2001) 291.
- [16] K.Y. Kim, H.G. Jung, B.G. Seong, S.Y. Hwang, *Oxid. Met.* 41 (1994) 12.
- [17] Z.G. Zgang, F. Gesmundo, P.Y. Hou, Y. Niu, *Corros. Sci.* 48 (2006) 741.
- [18] A.S. Khanna, *High Temperature Oxidation and Corrosion*, ASM International, Nevada, 2002 pp. 1–11.
- [19] J. Robertson, M.I. Manning, *Mater. Sci. Tech.* 5 (1989) 741.
- [20] N. Birks, G.H. Meier, *Introduction to High Temperature Oxidation of Metals*, Edward Arnold, London, 1983 pp. 73.